



# A finite-strain model for a superelastic NiTi shape memory alloy

Dongjie Jiang<sup>1</sup> , Yao Xiao<sup>2,3\*</sup> 

<sup>1</sup> School of Aeronautics and Astronautics, Shanghai Jiao Tong University, 200240 Shanghai, China.

<sup>2</sup> School of Mechanical Engineering, Tongji University, 201804 Shanghai, China.

<sup>3</sup> Institute for Advanced Study, Tongji University, 200092 Shanghai, China.

## Abstract

A finite-strain constitutive model of a superelastic NiTi shape memory alloy is proposed in this paper. Via backward Euler implicit integration scheme and the incorporation of material softening, the model is implemented into finite element code to reproduce a Lüders like deformation of a superelastic NiTi. The simulation results are in agreement with the experimental results, indicating that the constitutive model can reasonably predict the mechanical behavior of a superelastic NiTi. A parametric study further verifies that the magnitude of softening modulus has a significant effect on the stress-strain response and Lüders-like deformation of a superelastic NiTi.

**Keywords:** shape memory alloy, martensitic transformation, finite-strain constitutive model, Lüders-like deformation

## 1. Introduction

NiTi shape memory alloy (SMA) undergoes reversible martensitic transformation between austenite and martensite upon thermomechanical loading. When the deformation temperature is above the austenite finish temperature, NiTi demonstrates superelasticity with large recoverable transformation strain (up to 8%), high yielding stress (up to 1500 MPa) and appealing dissipation energy (up to 10 MJ/m<sup>3</sup>). In order to predict the complicated mechanical response of superelastic NiTi, constitutive modeling has been a research hot-spot in recent decades.

Starting from the early-stage 1-D phenomenological models proposed by Tanaka et al. (1986) and Liang & Rogers (1990), which adopted an exponential and cosine hardening rule for martensitic transformation respectively, numerous constitutive models have

been developed and continuously updated to deal with one or more aspects of the thermomechanical behavior of SMAs. Based on the framework of irreversible thermodynamics, Boyd & Lagoudas (1996) developed a 3-D phenomenological model of NiTi by decomposing the total free energy density into the free energy densities of the two phases weighted by the phase volume fractions in addition to a contribution from the mix of the two phases. The capability to depict different shapes of stress-strain response during martensitic transformation was established by unifying different forms of hardening functions (Lagoudas et al., 1996). To address the localized deformation during martensitic transformation, Abeyaratne & Knowles (1993) introduced a double-well potential function to account for the material instability, but its use is limited to 1-D problems and cannot describe the reverse transformation. Lubliner & Auricchio (1996) proposed

\*Corresponding author: xiaoy10@tongji.edu.cn

ORCID ID's: 0000-0001-9539-0440 (D. Jiang), 0000-0003-3011-8408 (Y. Xiao)

© 2022 Authors. This is an open access publication, which can be used, distributed and reproduced in any medium according to the Creative Commons CC-BY 4.0 License requiring that the original work has been properly cited.

a 1-D constitutive model for SMAs in which the single-variant martensite volume fraction is taken as the internal variable, and its evolution follows a flow rule confined by the transformation surfaces defined in the stress-temperature space. This model was later extended by Auricchio & Lubliner (1997) to 3-D with the addition of the reorientation of martensite. Panico & Brinson (2007) and Popov & Lagoudas (2007) took the stress-induced martensite fraction and the temperature-induced martensite fraction as separate internal variables and described martensite reorientation independently from austenite to martensite transformation. Hartl & Lagoudas (2009) extended this idea to include plastic yielding into the constitutive model of NiTi by adding a back stress term that governs the flow rule of plastic strain. Arghavani et al. (2010) presented a model in which the amount and orientation of the transformation strain evolve separately, and the two mechanisms inducing inelastic strains, i.e., transformation and reorientation, are decoupled. In order to reproduce the Lüders-like deformation of superelastic NiTi, Jiang et al. (2016, 2017a, 2017b), Xiao & Jiang (2020a) and Frost et al. (2018, 2021) developed several macroscopic constitutive models under isothermal condition by incorporating mechanical instability associated with martensitic transformation under primarily tensile stress states. Some of these models have been generalized to include thermomechanical coupling and grain size dependent of superelastic NiTi (Jiang & Xiao, 2021; Xiao & Jiang, 2020b). The issue of mesh dependency can be well addressed by involving an integral-type (Ahmadian et al., 2015) or gradient-enhanced non-locality (Hajidehi & Stupkiewicz, 2018; Hajidehi et al., 2020).

For the sake of simplicity, most of the constitutive models for superelastic NiTi are established based on the infinitesimal strain assumption, even though the transformation strain is about 7% (Cisse et al., 2016). For some special problems such as superelastic NiTi fracture, the strain level in the vicinity of crack tips may reach 10% or even higher (Haghgouyan et al., 2016, 2019; Jiang & Landis, 2016b). Consequently, developing a finite-strain constitutive model is vital in providing a physically-solid prediction. This paper proposes a finite-strain model to reproduce the stress-strain trace and Lüders-like deformation of superelastic NiTi. The model is implemented into finite element code via a backwards Euler implicit integration scheme. The origin of Lüders-like deformation is disclosed, and the effect of softening modulus on mechanical response is discussed numerically. The present study will offer new insights into the finite-strain modeling of NiTi and other phase transformable materials.

## 2. Constitutive model

### 2.1. Definition of strain

The initial configuration prior to deformation is denoted as the *reference configuration*  $\mathcal{R}$ , and the configuration after deformation is denominated as the *current configuration*  $\bar{\mathcal{R}}$ . From the Kroner–Lee decomposition, the total deformation gradient  $\mathbf{F}$  is decomposed as:

$$\mathbf{F} = \mathbf{F}^e \mathbf{F}^{tr} \quad (1)$$

where  $\mathbf{F}^e$  and  $\mathbf{F}^{tr}$  are the deformation gradients caused by elastic deformation and martensitic transformation, respectively. The total velocity gradient is defined as:

$$\mathbf{L} = \dot{\mathbf{F}}\mathbf{F}^{-1} \quad (2)$$

Substituting Equations (1) to (2), we get:

$$\mathbf{L} = \mathbf{L}^e + \mathbf{F}^e \mathbf{L}^{tr} \mathbf{F}^{e-1} \quad (3)$$

where  $\mathbf{L}^e = \dot{\mathbf{F}}^e \mathbf{F}^{e-1}$  and  $\mathbf{L}^{tr} = \dot{\mathbf{F}}^{tr} \mathbf{F}^{tr-1}$  are velocity gradients of elastic deformation and martensitic transformation, respectively. The Green–Lagrange strain tensors are expressed as:

$$\mathbf{E} = \frac{1}{2} (\mathbf{F}^T \mathbf{F} - \mathbf{I}) \quad (4)$$

$$\mathbf{E}^e = \frac{1}{2} (\mathbf{F}^{eT} \mathbf{F}^e - \mathbf{I}) \quad (5)$$

$$\mathbf{E}^{tr} = \frac{1}{2} (\mathbf{F}^{trT} \mathbf{F}^{tr} - \mathbf{I}) \quad (6)$$

The Martensite volume fraction yields:

$$\xi = \frac{E_{eq}^{tr}}{(E_{eq}^{tr})_{\max}} \quad (7)$$

where  $(E_{eq}^{tr})_{\max}$  is a material parameter reflecting the maximum transformation strain, which can be read as the maximum inelastic strain when martensitic transformation finishes in the stress-strain response during uniaxial tension.  $E_{eq}^{tr}$  is the equivalent transformation strain:

$$E_{eq}^{tr} = \left( \frac{2}{3} \mathbf{E}^{tr} : \mathbf{E}^{tr} \right)^{1/2} \quad (8)$$

### 2.2. Thermodynamic framework

The specific Helmholtz free energy of the material in *reference configuration*  $\mathcal{R}$  is divided as:

$$\psi = (1 - \xi)\psi^A + \xi\psi^M + \psi^m \quad (9)$$

where  $\psi^A$  and  $\psi^M$  are free energies of austenite and martensite, respectively.  $\psi^m$  is the free energy caused by

the martensitic transformation. Under the isothermal setting,  $\psi^A$  and  $\psi^M$  are written as:

$$\psi^X = \frac{1}{2} (S_{ijkl}^X)^{-1} E_{ij}^e E_{kl}^e \quad X = A, M \quad (10)$$

where  $A$  and  $M$  represent austenite and martensite, respectively.  $S_{ijkl}^X$  is the elastic compliance. The elastic property of each phase is supposed to be isotropic:

$$S_{ijkl}^X = \frac{1}{E_X} \left[ (1+\nu) I_{ijkl} - \nu \delta_{ij} \delta_{kl} \right] \quad X = A, M \quad (11)$$

where  $I_{ijkl} = (\delta_{ik} \delta_{jl} + \delta_{il} \delta_{jk}) / 2$  is fourth-order identity tensor,  $E_X$  is the elastic modulus, and  $\nu$  is Poisson's ratio. The effective elastic compliance is evaluated by the volume average of the elastic compliances of the two phases:

$$S_{ijkl} = (1-\xi) S_{ijkl}^A + \xi S_{ijkl}^M \quad (12)$$

Substituting Equations (10)–(12) into Equation (9), we get:

$$\psi = \frac{1}{2} (S_{ijkl})^{-1} E_{ij}^e E_{kl}^e + \psi^m \quad (13)$$

$\psi^m$  is decomposed as:

$$\psi^m = \psi^{mix} + \psi^{ind} \quad (14)$$

$\psi^{mix}$  originates from the austenite-martensite interfacial energy (Jiang & Xiao, 2021; Xiao & Jiang, 2020b):

$$\psi^{mix} = \alpha \xi (1-\xi) = \frac{H_1}{2} E_{eq}^{tr} \left[ (E_{eq}^{tr})_{\max} - E_{eq}^{tr} \right] \quad (15)$$

where  $H_1$  is the material parameter governing the interaction between austenite and martensite. In Equation (14),  $\psi^{ind}$  is the indicator energy finalizing martensitic transformation numerically when  $E_{eq}^{tr}$  approaches to  $(E_{eq}^{tr})_{\max}$ . The second law of thermodynamics in *reference configuration*  $\mathcal{R}$  is formulated as:

$$\Gamma = \left( \mathbf{T}^e - \frac{\partial \psi}{\partial \mathbf{E}^e} \right) : \dot{\mathbf{E}}^e + \mathbf{T}^{tr} : \mathbf{L}^{tr} - \frac{\partial \psi}{\partial \xi} \dot{\xi} \geq 0 \quad (16)$$

$$\mathbf{T}^e = \det(\mathbf{F}) \mathbf{F}^{e-1} \mathbf{T} \mathbf{F}^{e-T} \quad (17)$$

$$\mathbf{T}^{tr} = \det(\mathbf{F}) \mathbf{F}^{eT} \mathbf{T} \mathbf{F}^{e-T} \quad (18)$$

where  $\mathbf{T}$  is Cauchy stress. One should note the difference among  $\mathbf{T}^e$  in Equation (17),  $\mathbf{T}^{tr}$  in Equation (18) and the second Piola–Kirchhoff stress  $\mathbf{T}^{(1)} = \det(\mathbf{F}) \mathbf{F}^{-1} \mathbf{T} \mathbf{F}^{-T}$ , although they are defined in an apparently similar form. Since Equation (16) applies to all thermodynamic processes, we get:

$$\mathbf{T}^e = \frac{\partial \psi}{\partial \mathbf{E}^e} = S_{ijkl}^{-1} E_{kl}^e \quad (19)$$

In the vein of Equations (16)–(19), we get:

$$\Gamma = \left[ \mathbf{T}^{tr} - \mathbf{F}^{tr} \frac{\partial \psi^m}{\partial \mathbf{E}^{tr}} \mathbf{F}^{trT} + \mathbf{F}^{tr} \left( \frac{1}{2} \mathbf{T}^e : \frac{\partial \mathbf{S}}{\partial \mathbf{E}^{tr}} : \mathbf{T}^e \right) \mathbf{F}^{trT} \right] : \mathbf{L}^{tr} \geq 0 \quad (20)$$

For the sake of brevity and simplicity, we introduce the following definitions:

$$\mathbf{T}^B = \mathbf{F}^{tr} \frac{\partial \psi^m}{\partial \mathbf{E}^{tr}} \mathbf{F}^{trT} \quad (21)$$

$$\mathbf{T}^S = \mathbf{F}^{tr} \left( \frac{1}{2} \mathbf{T}^e : \frac{\partial \mathbf{S}}{\partial \mathbf{E}^{tr}} : \mathbf{T}^e \right) \mathbf{F}^{trT} \quad (22)$$

$$\hat{\mathbf{T}} = \mathbf{T}^{tr} - \mathbf{T}^B + \mathbf{T}^S \quad (23)$$

### 2.3. Transformation criterion

We recast Equation (21) according to the chain rule:

$$\mathbf{T}^B = T_B \mathbf{F}^{tr} \frac{\partial E_{eq}^{tr}}{\partial \mathbf{E}^{tr}} \mathbf{F}^{trT} \quad (24)$$

Referring to Xiao & Jiang (2020b),  $T_B$  can be expressed as:

$$T_B = T_s - H_1 E_{eq}^{tr} + \begin{cases} 0 & 0 \leq E_{eq}^{tr} < (E_{eq}^{tr})_{\max} - d \\ H_2 d (2.5\eta^4 - 3\eta^5 + \eta^6) & (E_{eq}^{tr})_{\max} - d \leq E_{eq}^{tr} \leq (E_{eq}^{tr})_{\max} \\ H_2 d (\eta - 0.5) & E_{eq}^{tr} > (E_{eq}^{tr})_{\max} \end{cases} \quad (25)$$

where  $T_s$  is the critical back stress at the onset of martensitic transformation.  $d$  is set as a sufficiently small constant ( $1 \times 10^{-4}$ ) and  $H_2$  an extremely large constant ( $2 \times 10^4$  GPa), as Xiao & Jiang (2020b) suggested. The transformation surface is assumed to be von Mises type, and the flowing rule is proposed to be:

$$\Phi = \frac{3}{2} \hat{\mathbf{t}} : \hat{\mathbf{t}} - \sigma_0^2 \quad (26)$$

$$\mathbf{L}^{tr} = \lambda \frac{\partial \Phi}{\partial \hat{\mathbf{T}}} \quad (27)$$

where  $\hat{\mathbf{t}}$  is the deviator of  $\hat{\mathbf{T}}$ ,  $\lambda$  is the multiplier, and  $\sigma_0$  is the size of the transformation surface.

## 3. Experimental setup

The NiTi sheet used in the experiment was purchased from Memry Corp. The austenite finish temperature is determined to be 11°C (Shuai & Xiao, 2020), indicating the material is superelastic at ambient temperatures (23°C).

The dog-bone specimen was machined from the sheet along the rolling direction. The thickness ( $t$ ), the gauge length ( $L$ ) and the gauge width ( $w$ ) are 1 mm, 8 mm and 2 mm respectively. The dimensions of the specimen are designed to make the gauge length much larger than the gauge width and thickness, accordingly the gauge section is under essentially uniaxial stress state. The tensile test is performed on an MTS testing machine at the strain rate of  $1 \times 10^{-4}$ /s to preclude thermomechanical coupling of superelastic NiTi. Stereo digital image correlation (DIC) is utilized to record the strain field of the sample throughout deformation.

terminated by half of the stress hysteresis. The softening modulus  $H_1$  adopted in the model is based on the one measured in the sandwich tensile test performed by Xiao et al. (2016). Material parameters are listed in Table 1.

**Table 1.** Material parameters of the numerical model

Elastic parameters			
$E_A = 60$ GPa	$E_M = 34$ GPa	$\nu = 0.3$	
Material parameters related to martensitic transformation			
$\epsilon'_{\max} = 0.06$	$\sigma_s = 230$ MPa	$H_1 = -1.5$ GPa	$\sigma_0 = 106$ MPa

## 4. Finite-element implementation

Via the backward Euler implicit integration scheme, the constitutive model is implemented into the ABAQUS user subroutine (UMAT). The size of the finite-element model is the same as the dog-bone sample used in the experiment, and it is discretized with 8960 C3D8I elements to get rid of mesh sensitivity. The mesh is shown in Figure 2a. The gauge section is meshed with uniform elements with size  $0.2 \text{ mm} \times 0.2 \text{ mm} \times 0.5 \text{ mm}$  such that there are 40, 10 and 2 elements in the longitudinal, transverse and through-the-thickness directions. The elements in the remaining parts have similar sizes. In order to reproduce the boundary conditions of the experimental setup, the vertical displacement is prescribed at the top of the numerical sample, whilst the other degrees of freedom of the top and bottom of the numerical sample are pinned.

The simulation results are calibrated with the tensile test of superelastic NiTi.  $E_A$  and  $E_M$  are measured by the elastic stress-strain division of austenite and martensite, respectively.  $\nu$  is set as 0.3.  $\epsilon'_{\max}$  is dictated by the maximum transformation strain.  $\sigma_s$  is evaluated by the back stress at the onset of transformation.  $\sigma_0$  is de-

## 5. Results and discussion

The stress-strain response and the evolution of the strain field obtained from the experiment are shown in Figure 1. The nominal stress is defined as the force divided by the initial cross-sectional area, and the global strain is defined as the extension of the gauge length divided by its initial value. The contours show the distribution of the nominal longitudinal strain within the gauge section. We can see that the deformation of superelastic NiTi is fulfilled by the propagation (Points 2 to 6) and retreating of the Lüders band (Points 8 to 11) at essentially constant stress, in accordance with the existing results (Kan et al., 2016; Kim & Daly, 2013; Shaw & Kyriakides, 1997; Xiao et al., 2017; Xie et al., 2016). Martensite concentrates primarily within the Lüders band, so the strain within the band is higher than 5% while the strain out of the band is less than 1.5%. When Lüders band is short (Points 2 and 11), its front takes the form of an inclined angle of about  $55^\circ$  to the loading axis, consistent with the theoretical analysis of Hill (1952). Whereas as Lüders band grows, its front becomes symmetric to the loading axis (Points 4, 5, 8 and 9), which was also observed by Xiao & Jiang (2020a).

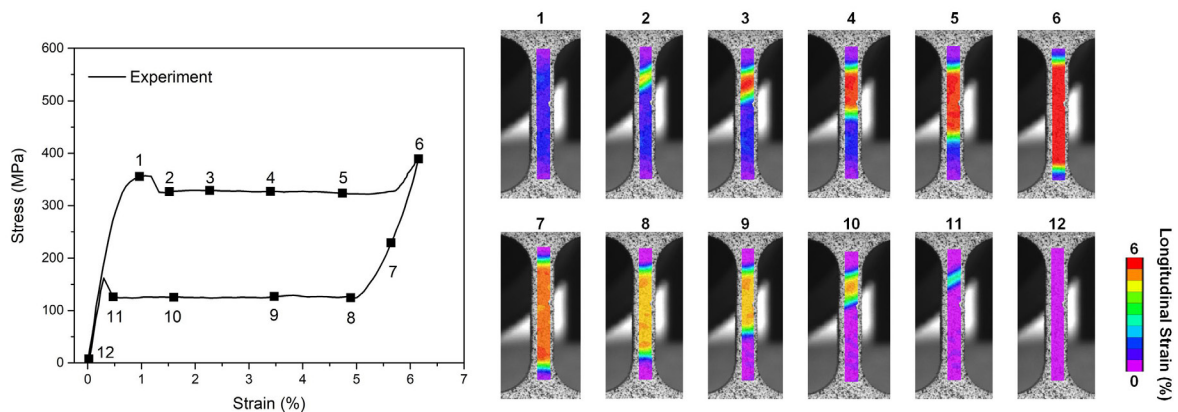


**Fig. 1.** Experimental results of the superelastic NiTi. The overall stress-strain response and the evolution of the strain field are provided

As reported in Hallai & Kyriakides (2013), the material softening during the martensitic transformation gives rise to the emergence of stress plateau and a Lüders-like deformation. From Figure 2, we can see that simulation can replicate the experimental measurement and observations reasonably, because negative  $H_1$  is involved in the constitutive model. The reasonably good agreement between the experimental and numerical stress-strain responses and deformation patterns shows that this constitutive model is effective. In future research, we will perform other experiments using the same material and simulate them to further validate the constitutive model.

In order to analyze the effect of softening modulus  $H_1$  on the numerical outcome, we vary the magnitude of  $H_1$  while keeping other characteristics of the intrinsic response similar. An overview of the simulated stress-strain response and strain field is illustrated in Figure 3a and Figure 4. As indicated by Figure 3b, when  $|H_1|$  increases, the local stress maximum prior to the stress plateau rises and the stress undulation of the stress plateau gets more evident. The comparison of strain fields in Figure 4 shows that the variation of  $|H_1|$  affects the Lüders-like deformation of the numerical model significantly, in terms of the shape of the Lüders band, the inclination

of the band front and the annihilation site of the Lüders band. When  $|H_1|$  equals to 2.0 GPa and 2.5 GPa, it is predicted that a crisscross appears in front of the band front (see the contours at 4% and 5% during loading or 3% and 4% during unloading), and the underlying mechanism requires further investigation. By contrast, as  $|H_1|$  decreases to 1.0 GPa and 0.5 GPa, the transition zone around the band front where the strain changes quickly from the large value above 5% to the small value below 1.5% becomes wider, and the band front becomes more visually diffused.

We also performed additional simulation by using a constitutive model we developed before (Jiang & Xiao, 2021) based on infinitesimal strain. The nominal stress-normalized elongation response and selected longitudinal strain contours simulated are plotted in Figure 5. The results from the infinitesimal strain model are not rather distinct from those based on finite deformation, because material points in a uniaxial tension specimen do not incur significant rigid body rotations for the difference to show up. However, a finite strain constitutive model is necessary for analysis under general loading conditions since the strain level of this material can deform up to over 10%, which is quite large and finite rotations may occur.

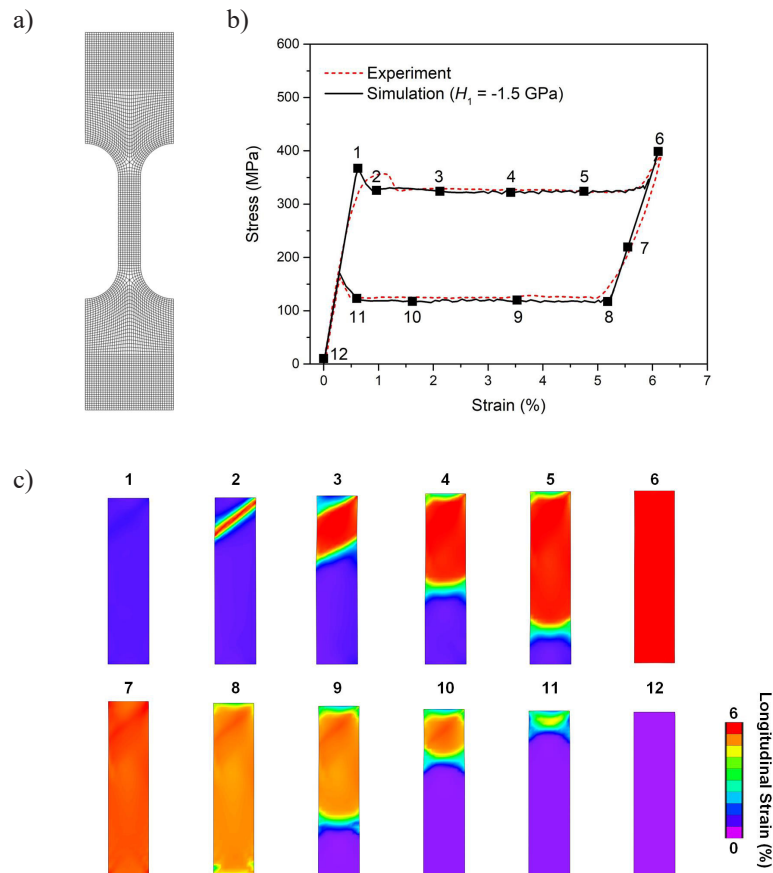


**Fig. 2.** Simulation results of superelastic NiTi ( $H_1$  is set as  $-1.5$  GPa according to Xiao et al. (2016)): a) front view of the FE mesh; b) the stress-strain response; c) the evolution of strain fields

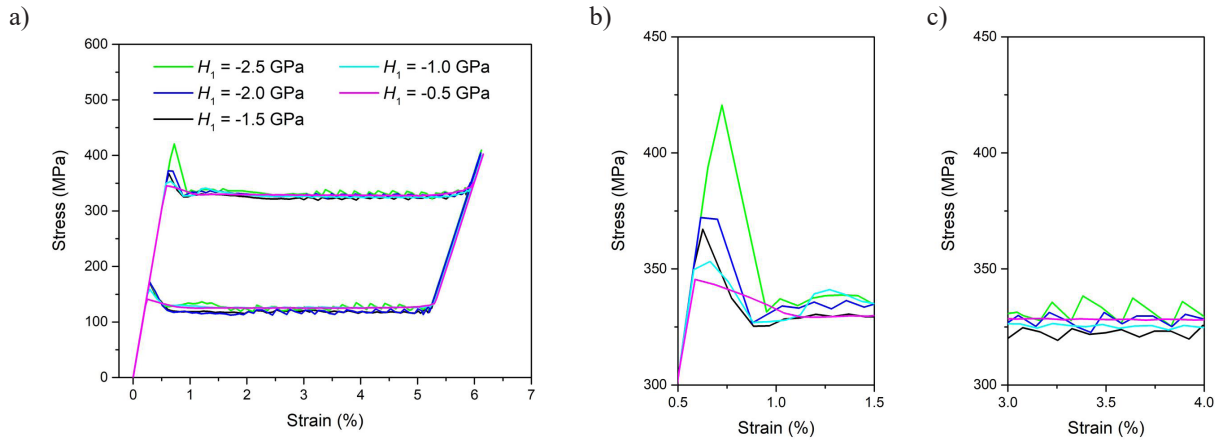


**Fig. 3.** The effect of  $H_1$  on the simulated stress-strain response of the numerical model: a) overview of stress-strain curves; b) enlarged stress-strain curves near local stress maximum during loading; c) enlarged stress-strain curves showing the stress undulation during loading

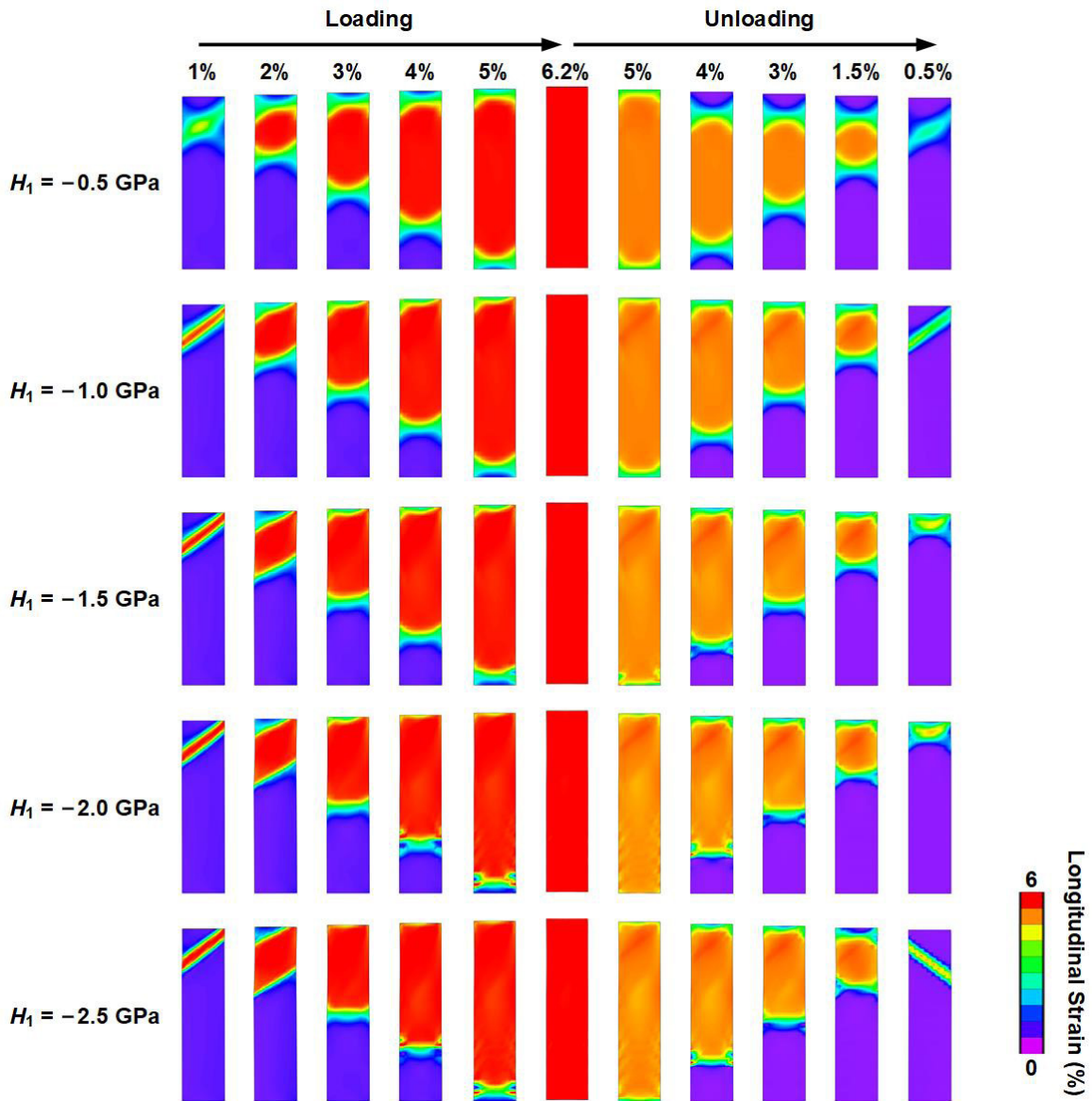


**Fig. 4.** The effect of  $H_1$  on the Lüders like deformation of the numerical model

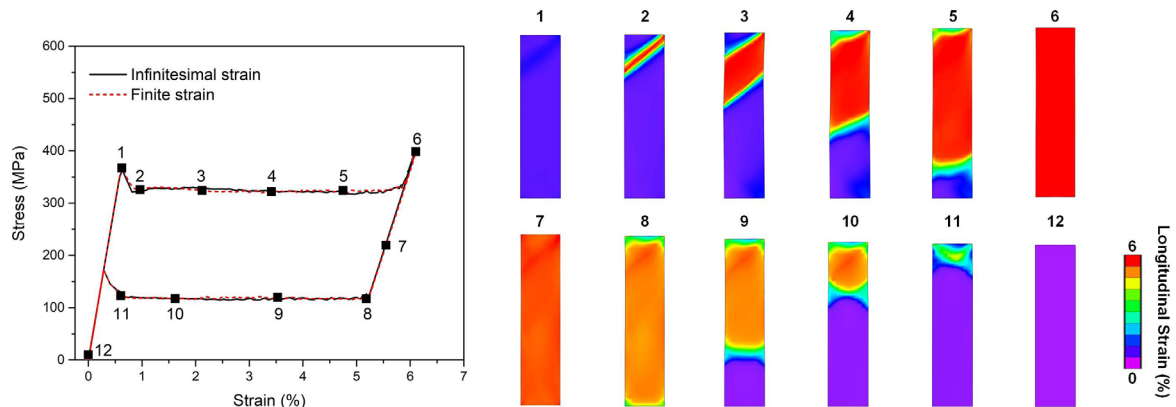


**Fig. 5.** Nominal stress-normalized elongation response and select strain contours of superelastic NiTi simulated using the model in Jiang & Xiao (2021) based on infinitesimal deformation

## 4. Conclusions

In this paper, a finite-strain constitutive model is proposed to reproduce the superelastic behavior of the NiTi shape memory alloy. The model is implemented into finite element code via a backwards Euler implicit integration scheme. The global mechanical response (e.g. stress-strain curve) and the local mechanical response (e.g. strain field) are simulated and verified with the experiment. The following conclusions can be drawn:

- Both the experiment and the simulation show that the deformation of the superelastic NiTi is fulfilled by a Lüders-like deformation. Numerical investigation indicates the emergence of the Lüders band is a consequence of material softening during martensitic transformation.

- A parametric study demonstrates that the magnitude of softening modulus  $|H_1|$  has a significant effect on the mechanical behavior of the superelastic NiTi. Increasing  $|H_1|$  gives rise to higher stress maxima and more evident stress undulation of stress plateau. It is anticipated that a crisscross will appear in front of the band front when  $|H_1|$  is above 2.0 GPa.

## Acknowledgement

Yao Xiao has been supported by the Shanghai Sailing Program (Grant No. 22YF1450600) and the Fundamental Research Funds for the Central Universities. Dongjie Jiang was sponsored by the National Natural Science Foundation of China (Grant No. 11902195).

## References

- Abeyaratne, R., & Knowles, J.K. (1993). A continuum model of a thermoelastic solid capable of undergoing phase transitions. *Journal of the Mechanics and Physics of Solids*, 41(3), 541–571.
- Ahmadian, H., Ardakani, S.H., & Mohammadi, S. (2015). Strain-rate sensitivity of unstable localized phase transformation phenomenon in shape memory alloys using a non-local model. *International Journal of Solids and Structures*, 63, 167–183.
- Arghavani, J., Auricchio, F., Naghdabadi, R., Reali, A., Sohrabpour, S. (2010). A 3-D phenomenological constitutive model for shape memory alloys under multiaxial loadings. *International Journal of Plasticity*, 26(7), 976–991.
- Auricchio, F., & Lubliner, J. (1997). A uniaxial model for shape-memory alloys. *International Journal of Solids and Structures*, 34(27), 3601–3618.
- Boyd, J.G., & Lagoudas, D.C. (1996). A thermodynamical constitutive model for shape memory materials. Part I. The monolithic shape memory alloy. *International Journal of Plasticity*, 12(6), 805–842.
- Cisse, C., Zaki, W., & Ben Zineb, T. (2016). A review of constitutive models and modeling techniques for shape memory alloys. *International Journal of Plasticity*, 76, 244–284.
- Frost, M., Sedláč, P., Sedmák, P., Heller, L., & Šittner, P. (2018). SMA constitutive modeling backed up by 3D-XRD experiments: transformation front in stretched NiTi wire. *Shape Memory and Superelasticity*, 4, 411–416.
- Frost, M., Benešová, B., Seiner, H., Kružík, M., Šittner, P., & Sedláč, P. (2021). Thermomechanical model for NiTi-based shape memory alloys covering macroscopic localization of martensitic transformation. *International Journal of Solids and Structures*, 221, 117–129.
- Haghgouyan, B., Shafaghi, N., Aydin, C.C., & Anlas, G. (2016). Experimental and computational investigation of the effect of phase transformation on fracture parameters of an SMA. *Smart Materials and Structures*, 25(7), 075010.

- Haghgouyan, B., Hayrettin, C., Baxevanis, T., Karaman, I., & Lagoudas, D.C. (2019). Fracture toughness of nitinol towards establishing standard test methods for phase transforming materials. *Acta Materialia*, *162*, 226–238.
- Hajidehi, M.R., & Stupkiewicz, S. (2018). Gradient-enhanced model and its micromorphic regularization for simulation of Lüders-like bands in shape memory alloys. *International Journal of Solids and Structures*, *135*, 208–218.
- Hajidehi, M.R., Tüma, K., & Stupkiewicz, S. (2020). Gradient-enhanced thermomechanical 3D model for simulation of transformation patterns in pseudoelastic shape memory alloys. *International Journal of Plasticity*, *128*, 102589.
- Hallai, J.F., & Kyriakides, S. (2013). Underlying material response for Lüders-like instabilities. *International Journal of Plasticity*, *47*, 1–12.
- Hartl, D.J., & Lagoudas, D.C. (2009). Constitutive modeling and structural analysis considering simultaneous phase transformation and plastic yield in shape memory alloys. *Smart Materials and Structures*, *18*(10), 104017.
- Hill, R.T. (1952). On discontinuous plastic states, with special reference to localized necking in thin sheets. *Journal of the Mechanics and Physics of Solids*, *1*(1), 19–30.
- Jiang, D., & Landis, C.M. (2016). A constitutive model for isothermal pseudoelasticity coupled with plasticity. *Shape Memory and Superelasticity*, *2*(4), 360–370.
- Jiang, D., & Xiao, Y. (2021). Modelling on grain size dependent thermomechanical response of superelastic NiTi shape memory alloy. *International Journal of Solids and Structures*, *210–211*, 170–182.
- Jiang, D., Landis, C.M., & Kyriakides, S. (2016). Effects of tension/compression asymmetry on the buckling and recovery of NiTi tubes under axial compression. *International Journal of Solids and Structures*, *100–101*, 41–53.
- Jiang, D., Kyriakides, S., Bechle, N.J., & Landis, C.M. (2017a). Bending of pseudoelastic NiTi tubes. *International Journal of Solids and Structures*, *124*, 192–214.
- Jiang, D., Kyriakides, S., Landis, C.M., & Kazinakis, K. (2017b). Modeling of propagation of phase transformation fronts in NiTi under uniaxial tension. *European Journal of Mechanics – A/Solids*, *64*, 131–142.
- Kan, Q., Yu, C., Kang, G., Li, J., & Yan, W. (2016). Experimental observations on rate-dependent cyclic deformation of super-elastic NiTi shape memory alloy. *Mechanics of Materials*, *97*, 48–58.
- Kim, K., & Daly, S. (2013). The effect of texture on stress-induced martensite formation in nickel–titanium. *Smart Materials and Structures*, *22*(7), 075012.
- Lagoudas, D.C., Bo, Z., & Qidwai, M.A. (1996). A unified thermodynamic constitutive model for SMA and finite element analysis of active metal matrix composites. *Mechanics of Composite Materials and Structures*, *3*(2), 153–179.
- Liang, C., & Rogers, C.A. (1990). One-dimensional thermomechanical constitutive relations for shape memory materials. *Journal of Intelligent Material Systems and Structures*, *1*(2), 207–234.
- Lubliner, J., & Auricchio, F. (1996). Generalized plasticity and shape memory alloys. *International Journal of Solids and Structures*, *33*(7), 991–1003.
- Panico, M., & Brinson, L.C. (2007). A three-dimensional phenomenological model for martensite reorientation in shape memory alloys. *Journal of the Mechanics and Physics of Solids*, *55*(11), 2491–2511.
- Popov, P., & Lagoudas, D.C. (2007). A 3-D constitutive model for shape memory alloys incorporating pseudoelasticity and detwinning of self-accommodated martensite. *International Journal of Plasticity*, *23*(10–11), 1679–1720.
- Shaw, J.A., & Kyriakides, S. (1997). On the nucleation and propagation of phase transformation fronts in a NiTi alloy. *Acta Materialia*, *45*(2), 683–700.
- Shuai, J., & Xiao, Y. (2020). In-situ study on texture-dependent martensitic transformation and cyclic irreversibility of super-elastic NiTi shape memory alloy. *Metallurgical and Materials Transactions A*, *51*(2), 562–567.
- Tanaka, K., Kobayashi, S., & Sato, Y. (1986). Thermomechanics of transformation pseudoelasticity and shape memory effect in alloys. *International Journal of Plasticity*, *2*(1), 59–72.
- Xiao, Y., & Jiang, D. (2020a). Constitutive modelling of transformation pattern in superelastic NiTi shape memory alloy under cyclic loading. *International Journal of Mechanical Sciences*, *182*, 105743.
- Xiao, Y., & Jiang, D. (2020b). Rate dependence of transformation pattern in superelastic NiTi tube. *Extreme Mechanics Letters*, *39*, 100819.
- Xiao, Y., Zeng, P., & Lei, L. (2016). Experimental investigation on the mechanical instability of superelastic NiTi shape memory alloy. *Journal of Materials Engineering and Performance*, *25*(9), 3551–3557.
- Xiao, Y., Zeng, P., Lei, L., & Zhang, Y. (2017). In situ observation on temperature dependence of martensitic transformation and plastic deformation in superelastic NiTi shape memory alloy. *Materials & Design*, *134*, 111–120.
- Xie, X., Kan, Q., Kang, G., Lu, F., & Chen, K. (2016). Observation on rate-dependent cyclic transformation domain of super-elastic NiTi shape memory alloy. *Materials Science and Engineering: A*, *671*, 32–47.